THE JOURNAL OF PHYSICAL CHEMISTRY C

Article

pubs.acs.org/JPCC

DFT-D3 Study of Molecular N_2 and H_2 Activation on Co_3Mo_3N Surfaces

Constantinos D. Zeinalipour-Yazdi,*,† Justin S. J. Hargreaves,‡ and C. Richard A. Catlow*,†

†Kathleen Lonsdale Materials Chemistry, Department of Chemistry, University College London, London, WC1H 0AJ, United Kingdom

‡WestCHEM, School of Chemistry, Joseph Black Building, University of Glasgow, Glasgow G12 8QQ, United Kingdom

ABSTRACT: Cobalt molybdenum nitride (Co_3Mo_3N) is one of the most active catalysts for ammonia synthesis, although the atomistic details of the reaction mechanism are currently unknown. We present a dispersion-corrected (D3) DFT study of the adsorption and activation of molecular nitrogen and hydrogen on Co_3Mo_3N-(111) surfaces to identify possible activation sites for ammonia synthesis. H_2 was found to adsorb both molecularly on the Mo_3N framework and dissociatively on Co_8 clusters or Mo_3 clusters that were exposed due to N-vacancies. We find that there are two possible activation sites for N_2 where both N_2 and H_2 can coadsorb. The first is a Mo_3 triangular cluster that resides at 3f nitrogen vacancies, and the second is a surface cavity where N_2 is activated by a Co_8 cluster, the second being a more efficient activation site. N_2 was found to adsorb in three adsorption configurations: *side-on*, *end-on*, and an unusual *tilt end-on* (155°) configuration, and the existence of these three adsorption configurations is explained via MP2 calculations and the sphere-in-contact model.

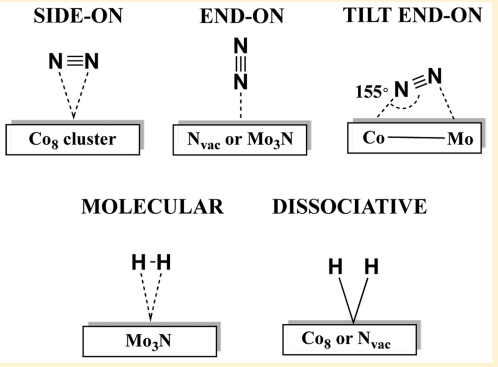

1. INTRODUCTION

Co_3Mo_3N when synthesized using the procedure patented by Topsøe[1] is known to be active for ammonia synthesis at 400 °C and elevated pressures using a 3:1, H_2:N_2 mixture.[2,3] Indeed, Co_3Mo_3N when doped with Cs is one of the most active catalysts for ammonia synthesis,[2,4] with turnover-frequencies (TOF) that are remarkably high compared to graphite-supported Ru and Fe−K_2O−Al_2O_3, the two catalysts currently used industrially for large scale ammonia synthesis.[2−8] Linear quantitative structure−property relationships (QSPR) between the dissociation energy of N_2 and its adsorption energy on Co_3Mo_3N were derived via periodic planewave DFT calculations[5,9] and the barrier for N_2-dissociation was found to be the rate-determining step (RDS). It has been previously suggested that ammonia synthesis may proceed via Mars−van Krevelen (MvK) chemistry and that lattice nitrogen may act in nitrogen transfer,[10] which was also confirmed by isotopic-exchange studies that showed that the lattice-N in Co_3Mo_3N is exchangeable at elevated temperatures.[11] The chemistry of N_2/H_2 with Co_3Mo_3N has been previously studied via two experiments, which showed that such materials can be used as reagents to produce ammonia, consuming nitrogen that originates from the *bulk* of these materials.[12] These experiments confirm the gas phase nitrogen exchangeability with lattice-N based on powder XRD and isotopic studies.[11] They also showed that the Co_3Mo_3N can be regenerated from a less nitrogen-rich phase (i.e., Co_6Mo_6N) via a 700 °C reaction with N_2/H_2 or even N_2, whereas the reverse reaction was obtained by changing the feedstream to Ar/H_2. We have recently shown via DFT calculations that the mechanism can also proceed via MvK type *surface* chemistry at low temperatures as there is a large number of nitrogen vacancies (~10^{13} cm^{-2}), which can activate N_2 by weakening of the triple bond.[13] N-vacancies were also found to participate in the mechanism for the electrochemical reduction of ammonia on VN and ZrN[14] and in the two-step solar-energy driven ammonia synthesis on metal nitrides.[15,16] Here, we extend the earlier study by investigating the adsorption at every possible site compared to the adsorption of molecular hydrogen.

The rest of the paper has the following structure: first we establish the calculation parameters that reproduce well the electronic structure of $Fe_xCo_{(3-x)}Mo_3N$, where x = 0, 1, 2 and 3; next we describe the method for generating slabs of Co_3Mo_3N-(111) surfaces and apply the calculation parameters to address the question of hydrogen and nitrogen adsorption and activation on Co_3Mo_3N with and without defects. Finally we explain the various bonding configurations of N_2 via molecular orbital (MO) calculations and the sphere-in-contact model.

2. COMPUTATIONAL METHODS

2.1. Methodology. Spin-polarized periodic planewave calculations have been performed with the VASP 5.3.5[17,18] code using the revPBE[19] and a 650 eV cutoff for the planewave

Received: May 28, 2016
Revised: August 23, 2016
Published: August 24, 2016

DOI: 10.1021/acs.jpcc.6b04748
J. Phys. Chem. C 2016, 120, 21390−21398

Table 1. Experimental and Calculated Lattice Parameter in Angstroms for 2 × 2 × 2 $Fe_{(3-x)}Co_xMo_3N$, (x = 0, 1, 2, 3), and Their Corresponding Average MAPE Using the revPBE Functional at 650 eV and a 11 × 11 × 11 MP k-Point Mesh

XC	Fe_3Mo_3N (Å)	Fe_2CoMo_3N (Å)	$FeCo_2Mo_3N$ (Å)	Co_3Mo_3N (Å)	$MAPE_1$[a] (%)	$MAPE_2$ (%)
PBE	11.072	11.055	10.999	11.076	0.36	0.30
revPBE	11.150	11.153	11.029	11.077	0.55	0.50
PBE_{sol}	10.869	10.864	10.867	10.864	1.61	1.77
PW91	10.997	10.979	11.002	10.994	0.51	0.61
Exp_1	11.0910[25]	11.0661[26]	11.0315[25]	10.9808[27]		
Exp_2[28]	11.0843	11.0708	11.0556	11.0297		

[a]Average MAPE calculated based on ref 13.

expansion. A detailed description of the computational methodology for the planewave calculations can be found in ref 13, in which it was found that among various GGA and hybrid-GGA XC functionals, the revPBE yields accurate (to within 1%) bond dissociation enthalpies for $N_2(g)$. Here, we further test how well this functional can perform in modeling correctly the electronic structure in a homologous series $Fe_{(3-x)}Co_xMo_3N$, (x = 0, 1, 2, 3), via reproducing the lattice parameters when compared to powder neutron-diffraction (PND) data. The adsorption energy was taken in its simplest form, as the energetic difference between the total energies of the bound state of the surface−adsorbate complex from that of the surface slab and the isolated molecules, the latter in a 20 Å periodic unit cell, given by

$$\Delta E_{ads,D3} = E_{slab-X2} - E_{slab} - E_{X2} \quad (1)$$

where X = N, H. The adsorption energy was also corrected for the dispersion correction using two approaches via the DFT-D3 method as implemented in VASP.[20] The first ($\Delta E_{ads,D3relax}$) was to fully relax the cluster-adsorbate system, the surface and the adsorbate separately. The second was by performing a single point energy calculation with the D3-correction at the minimum energy structure obtained from an optimization without the correction ($\Delta E_{ads,D3static}$). We find that the latter can lead to large errors with respect to the adsorption energies of hydrogen, which was overestimated by 35% in some cases and have therefore applied the former approach.

Molecular calculations for the electronic structure of N_2 were performed within restricted density functional theory (DFT) implemented in the Gaussian09 code (rev D.01).[21] The basis set used was the correlation-consistent polarized valence double-ζ abbreviated as cc-pVDZ.[22] Stationary states were confirmed by the absence of imaginary frequencies in the vibrational analysis. The convergence criteria for the maximum forces and the root-mean-square (RMS) forces were less than 0.01 eV/Å and 0.001 eV/Å, respectively.

2.2. Choice of XC-Functional for $Fe_xCo_{(3-x)}Mo_3N$. We find that the choice of exchange-correlation (XC) functional is critical when addressing the chemistry of N_2/H_2 with $Fe_xCo_{(3-x)}Mo_3N$, where x = 0, 1, 2, and 3. Although it has been shown for solids that hybrid XC functionals HSE03[23] (HSE06[24]) and PBE0 give better results for calculating lattice parameters, bulk moduli and more importantly formation enthalpies, for cobalt and iron molybdenum nitrides and their alloys; we note that the revPBE functional, which is computationally far less demanding than PBE0 and HSE03/06 can yield an accurate description of the electronic structure of the material under study. Furthermore, it does not overestimate the bandgap by overestimation of the exchange splitting known for the hybrid functional PBE0.[23] It has been suggested that the HSE06 functional greatly improves the computer time and resource requirements mostly due the faster convergence of the total energy with respect to k-point mesh, as the bare unscreened exchange operator requires a 12 × 12 × 12 mesh equivalent to a 6 × 6 × 6 mesh for the HSE06 functional.[23] However, we found that the latter underestimates by 38 kJ/mol the bond dissociation enthalpy of $N_2(g)$, $\Delta_{0K}H(N-N)$. Therefore, we have tested the remaining XC-functionals commonly used for solids, PBE, PW91, revPBE, and PBEsol with respect to their accuracies in predicting the lattice constant of $Fe_xCo_{(3-x)}Mo_3N$, where x = 0, 1, 2, and 3 (see Table 1). These alloys contain also iron which makes possible the testing of the computational methodology on other elements for which crystallographic data are available.[25−27] Our calculations are based on full optimization of unit cell dimensions and atom positions and the reported mean-average-percent-error (MAPE) value, which indicates to within which percentage the experimental values, are reproduced. The calculated values were compared to two sets of experimental lattice constants: the first comprised solely of PND data obtained at 4.2K (Exp_1) and the second based on combined XRD and temperature-dependent magnetic susceptibility measurements (Exp_2). In both sets, we obtained the same trend with respect to the average-MAPE calculated at each functional, which was found to be PBE < revPBE ≈ PW91 < PBEsol. In particular, according to Table 1, an average MAPE of 0.30−0.36% was found for PBE: both revPBE and PW91 gave values of about 0.5−0.6% and PBEsol gave higher average MAPE, of the order of 2%. The results show that with the use of a planewave code the lattice parameter can be estimated very well both with the PBE and the revPBE functional, which are also computationally less expensive than some of the hybrid GGA functionals tested.

In an earlier account of bond dissociation enthalpy (BDE) of N_2 with the use of various XC functional, the % error for the revPBE was found to be the lowest among various GGA and hybrid GGA functionals.[13] In particular, we found that the % error was for revPBE = 0.2 < B3LYP = 1.7 < PBE0 = 3.5 < HSE06 = 4.1 < PBE = 4.9 < PW91 = 7.0. Therefore, all subsequent calculations have been performed with the revPBE functional, which can yield more accurate barrier heights according to the calculated BDE of the N≡N bond.

3. RESULTS AND DISCUSSION

3.1. Surface Models of Co_3Mo_3N. We have modeled the surface of Co_3Mo_3N using a 2 × 2 supercell slab with trigonal symmetry belonging to the space group $P\bar{3}m1$ (164), where a = b = 7.7972 Å, c = 30 Å, α = β = 90°, and γ = 120°. This was generated from a cubic unit cell with the η-carbide Fe_3W_3C structure belonging to the space group $Fd\bar{3}m$ (227), where a =

DOI: 10.1021/acs.jpcc.6b04748
J. Phys. Chem. C 2016, 120, 21390−21398

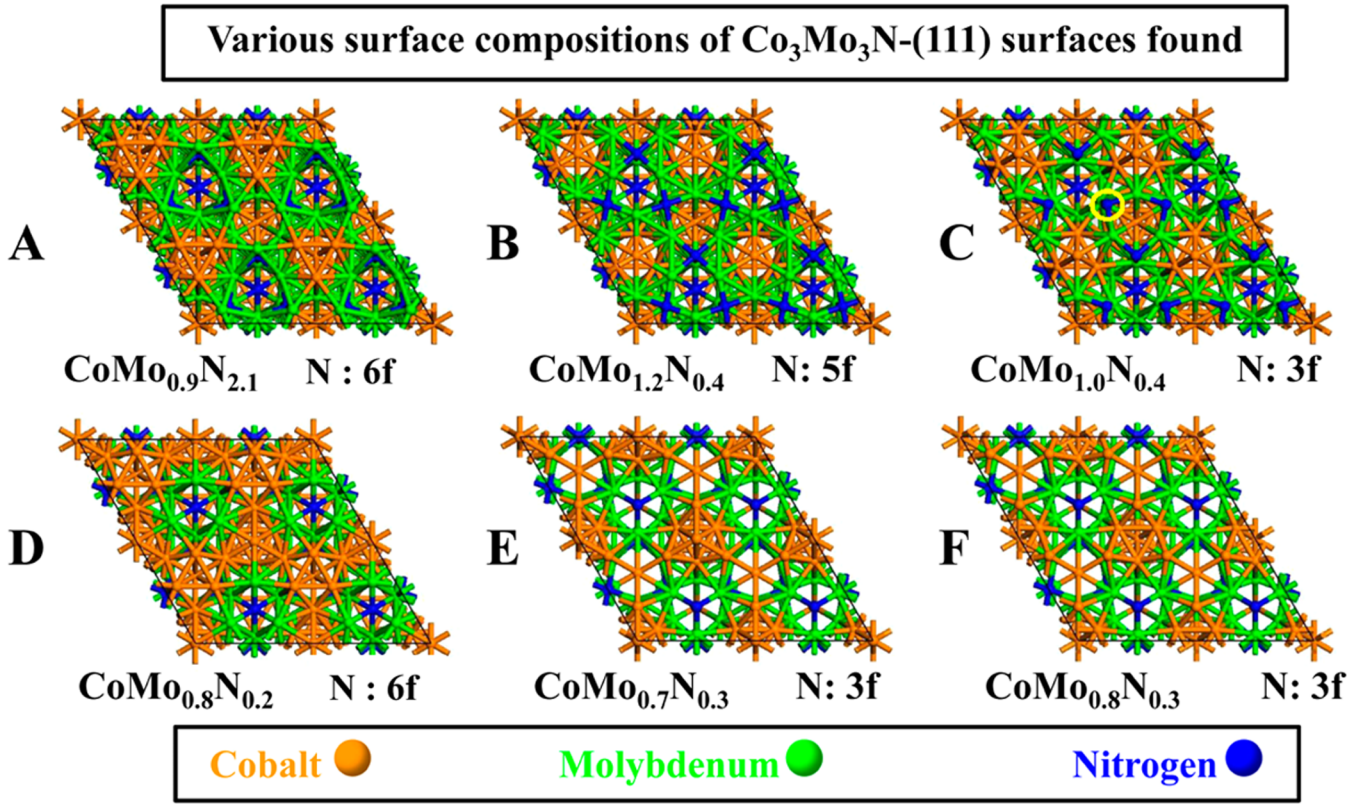

Figure 1. 2 × 2 surface supercells of Co_3Mo_3N showing surface terminations of different composition in cobalt molybdenum nitride (111) surfaces. Note that only four out of the six surface compositions expose surface nitrogen (i.e., 5f or 3f). Two surfaces only have subsurface nitrogen (i.e., 6f).

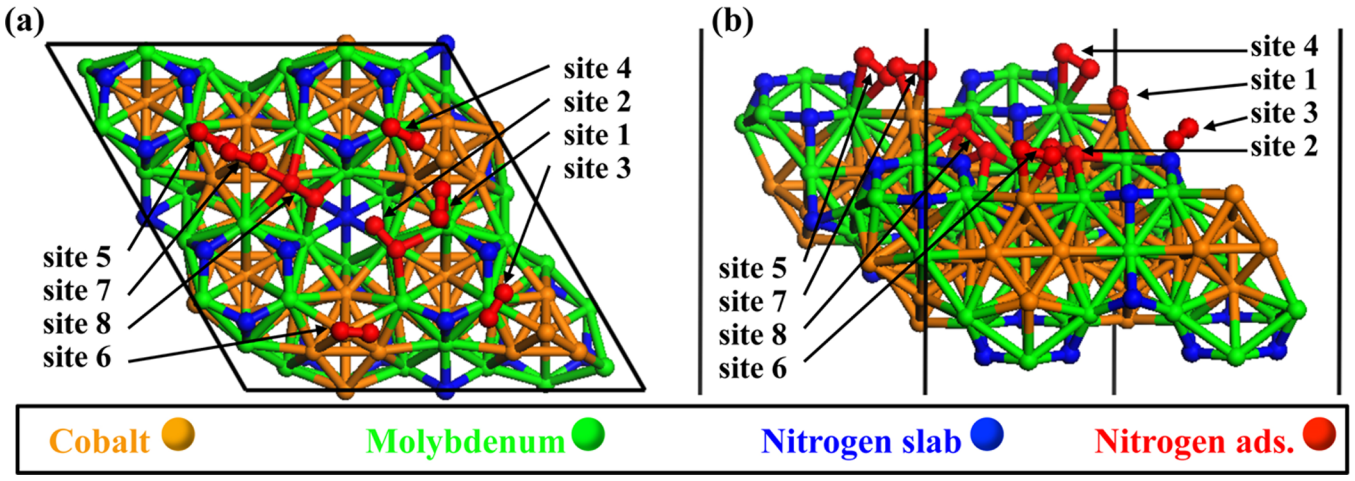

Figure 2. Symmetry unique sites for molecular hydrogen adsorption on Co_3Mo_3N surface C, in the presence of a nitrogen vacancy (**site 1** and **2**) in (a) top view and (b) perspective view.

$b = c = 11.0270$ Å and $\alpha = \beta = \gamma = 90°$.[29] We note that the (111) surface of the cubic unit cell ($Fd\bar{3}m$) is the (001) surface of the trigonal unit cell ($P\bar{3}m1$), which was further studied as it has the highest density of Co_8 clusters embedded in a molybdenum nitride (Mo_3N) framework. In the case of a bifunctional mechanism, this surface would have the largest density of active sites. For the rest of the paper, we refer to this "(111)-surface" simply as "surface". Note that the actual 2 × 2 supercell used for these periodic slab calculations was shifted by $a/2$ and along a and by $b/2$ along b and had a nitrogen vacancy at the position indicated by a yellow circle in Figure 1. The slabs were generated by applying a scanning algorithm to scan the bulk in 0.1 Å increments and generate centro-symmetric slabs of thickness <1 nm for computational efficiency. A top view of these slabs along the c direction is shown in Figure 1 that shows the composition of six distinct surfaces generated, of which four had surface nitrogen (i.e., **B**, **C**, **E**, and **F**) and two had only a MoCo exposed phase (i.e., **A** and **D**) with subsurface nitrogen. The subsurface nitrogen is a 6-fold bound nitrogen (6f) to Mo atoms, whereas surfaces **C**, **D**, and **F** had entirely 3f nitrogens, and one surface (**B**) had 5f nitrogens. The nitrogen vacancy formation energies (VFE) and concentrations have been previously calculated, and the latter was found to be on the order of 10^{13} per cm^2 at ambient conditions.[13] We have

DOI: 10.1021/acs.jpcc.6b04748
J. Phys. Chem. C 2016, 120, 21390−21398

evaluated the surface composition in these slabs and found that it significantly differs among these thin films. It is interesting to note that the surface with the highest surface nitrogen concentration, **C** had a very low composition of nitrogen based on the normalized stoichiometric coefficient (s.c.) of nitrogen, having set the s.c. of cobalt to 1. These compositions were found to be **A** = $CoMo_{0.9}N_{2.1}$, **B** = $CoMo_{1.2}N_{0.4}$, **C** = $CoMo_{1.0}N_{0.4}$, **D** = $CoMo_{0.8}N_{0.2}$, **E** = $CoMo_{0.7}N_{0.3}$, and **F** = $CoMo_{0.8}N_{0.3}$. For example surface **A**, which had a complete absence of exposed surface nitrogens, had the highest stoichiometric coefficient for nitrogen (i.e., $N_{2.1}$). This suggests that the exact surface composition of very thin layers of this material may have to be evaluated by topographic techniques, e.g., via scanning probe microscopies that are currently absent in the literature. In an earlier DFT study[13] with the same methodology used here, we proposed that surface **C** is the most active surface for Mars−van Krevelen type chemistry for ammonia synthesis. This choice was based on two kinetic factors and an energetic factor: (i) the density of sites that can activate N_2 (i.e., N-vacancies), (ii) which surface had the most exothermic adsorption energies for N_2 adsorption, and (iii) the surface formation energies (E_S^F), which were calculated for the four surface compositions that had exposed surface nitrogen. As the calculation of surface stabilities is not possible for Co_3Mo_3N, we continue with surface **C** for calculating the coadsorption of N_2/H_2 on Co_3Mo_3N.

3.2. H_2 Adsorption and Activation on Co_3Mo_3N.

Various phases of atomically adsorbed hydrogen have been observed via scanning-tunnelling microscopy (STM) on Co nanoparticles grown on Cu(111).[30] In a recent DFT study, the adsorption energy of H_2 was found to be roughly proportional to the surface energy in the following order Co(100) > Co(110) > Co(111).[31] The nitrogen vacancy-induced heterogeneity of the surface, offers H_2 an additional degree of complexity with respect to the availability of adsorption sites. In this study, we have studied the adsorption of H_2 at 8 symmetry unique sites of the **C** surface of Co_3Mo_3N shown in Figure 2, with a nitrogen vacancy shown by the yellow circle in Figure 1. This surface is expected to yield a better representation of the actual surface of the catalyst, which we have previously shown to have a large number of nitrogen vacancies ($\sim 10^{13}$ cm^{-2}) even at ambient temperature. The adsorption energy of H_2 was found to be roughly proportional to the percentage of H−H activation defined as the percentage lengthening of the H−H bond, when adsorbed side-on at every adsorption site with an adsorption angle of a(M−H−H) = 72°−87°. In this adsorption configuration, the adsorbate−surface bonding is interpreted as an interaction between the filled 1σ MO of H_2 with empty π-states of the metal and π-back-donation into the antibonding orbital of H_2. Interestingly an end-on adsorption could not be found in agreement with H_2 adsorption studies on rhodium clusters.[32] H_2 can absorb either *molecularly* or *dissociatively* (see Scheme 1) at five distinct adsorption sites after optimization of 8 symmetry unique adsorption sites, which are shown in Figure 2. The molecular adsorption occurred mostly on the MoN_3 framework, where it was bound through the Mo atoms (see Table 2). Dissociative adsorption occurred on exposed Co atoms that belong to the Co_8 clusters or Mo_3 clusters that were exposed due to N-vacancies.

Scheme 1. Simplified Schematic Showing (a) *Molecular* and (b) *Dissociative* Adsorption of H_2 on Co_3Mo_3N Surfaces

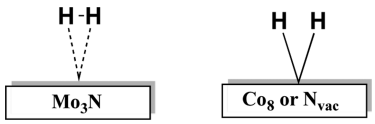

The adsorption energies without (ΔE_{H2}) and with ($\Delta E_{H2,relax\text{-}D3}$, $\Delta E_{H2,static\text{-}D3}$) the inclusion of dispersion interactions via the DFT-D3 method and the optimized structure of the adsorbates (i.e., $r_{(H-H)}$, $r_{(M-H)}$, $a_{(M-H-H)}$) are presented in Table 2. We have also calculated % activation, defined as the percent increase of the H−H bond length during adsorption. It may seem at some point surprising that the addition of the D3 correction can shift the adsorption energy endo- or exothermically; however, for the static calculation, it always adds to a more exothermic adsorption energy, which is what is expected.

The various adsorption sites found had the following characteristics: **site 1** the hydrogen was adsorbed side-on to a molybdenum atom that was adjacent to a nitrogen-vacancy site ($\mathbf{N_{vac}}$) with an adsorption energy of −67 kJ/mol but with only a small activation of the H−H bond.

Site 2 was found to dissociatively chemisorb H_2, where it was bound to a molybdenum atom at a nitrogen vacancy site. This site had the largest % activation (i.e., 41%) for molecular hydrogen; **sites 3−5** in which hydrogen was adsorbed on a molybdenum atom on the MoN_3 framework with a moderate adsorption energy of −30 to −68 kJ/mol due to the less metallic character of the MoN_3 framework. The strongest adsorption energy for H_2 was found on **sites 6−7**, which corresponds to a corner atom of the Co_8 nanoclusters denoted as $\mathbf{Co_{8\text{-}top}}$, with adsorption energy of −127 and −110 kJ/mol, respectively. At these sites, the H−H bond was also found to be considerably activated (i.e., 23−24%). These results indicate that the Co_8 clusters will be saturated with molecular hydrogen at low temperatures under conditions where both N_2/H_2 are available in the feedstream. Interestingly we find that at **site 8**, H_2 will generally not adsorb at low-T based on the D3-corrected adsorption energy of just 21 kJ/mol, and it is the only site on the Co_3Mo_3N surface that will not be occupied by hydrogen when it is coadsorbed with N_2. Therefore, we consider **site 8** as free under conditions of competitive adsorption with N_2 at low temperatures (e.g., T < 200 °C).

3.3. N_2 Adsorption and Activation on Co_3Mo_3N.

The adsorption of N_2 over a range of surfaces has been studied using various surface analytical probes extensively. Both physisorbed and chemisorbed states are identified using a combination of electron spectroscopy and thermal desorption techniques.[33] According to this report and earlier LEED experiments, N_2 can chemisorb *side-on* and *end-on* on the surfaces of certain metals (e.g., Ni, Fe, Ru, and W). In this study, we find that apart from these two adsorption configurations, N_2 can also adsorb in a *tilt end-on* configuration on Co_3Mo_3N shown in Scheme 2. This is a well-defined adsorption configuration with a tilt angle equal to 155° in which the dihedral d(Co−Mo−N−N) of this bond is found to be 0°.

Angle resolved photoemission spectra have identified two phases of N_2 adsorbed to Fe(111) surfaces (γ-phase and α-phase). In the first, N_2 is adsorbed perpendicularly, and in the latter in a strongly inclined configuration, where N_2 was described to form two covalent bonds with Fe atoms.[34] A c(2 × 2)-N/Fe(100) structure was found to form on Fe(111) and Fe(110) surfaces, whereas two *side-on* (α and α') and two *end-on* (β and γ) adsorbed states have been found via periodic DFT calculations for molecular N_2 adsorption on Fe(111).[35] Two

DOI: 10.1021/acs.jpcc.6b04748
J. Phys. Chem. C 2016, 120, 21390−21398

Table 2. Adsorption Energy (ΔE) of H_2 Adsorbed to C Surface of Co_3Mo_3N; H−H Bond Length (r(H−H)), M−N Bond Length (r(M−H)); Tilt Angle (a(M−H−H)), Adsorption Site Composition and % Elongation for *Side-On* Adsorption at Various Distinct Adsorption Sites on 2 × 2 Co_3Mo_3N with a Slab Composition of $CoMoN_{0.4}$[a]

property	site 1	site 2	site 3	site 4	site 5	site 6	site 7	site 8	units
ΔE_{H2}	−78	−88	−50	−65	−64	−125	−124	49	kJ/mol
$\Delta E_{H2,\ relax\text{-}D3}$	−67	−96	−30	−55	−68	−127	−110	21	kJ/mol
$\Delta E_{H2,\ static\text{-}D3}$	−106	−146	−71	−91	−92	−139	−136	−1	kJ/mol
r(H−H)	0.826	1.041	0.768	0.809	0.807	0.910	0.917	0.800	Å
a(M−H−H)	79	72	85	79	80	73	73	87	°
r(M−H)	1.971	1.779	2.195	2.013	2.002	1.577	1.578	2.377	Å
type	side-on	side-on	side-on	side-on	side-on	side-on	side-on	side-on	
bound to	N_{vac}	N_{vac}	MoN_3	MoN_3	MoN_3	$Co_{8\text{-}top}$	$Co_{8\text{-}top}$	$Co_{8\text{-}side}$	
H_2 activation[b]	12	41	4	9	9	23	24	8	%

[a]The *32e* and *16d* Wyckoff sites of the Co_8 in the bulk, have been denoted as $Co_{8\text{-}top}$ and $Co_{8\text{-}side}$ for the surface slabs, respectively. [b]Percent activation is defined as $[r(H_2,g) - r(H_2,ads)] \times 200/[r(H_2,g) + r(H_2,ads)]$.

Scheme 2. Simplified Schematic Showing *Side-On*, *End-On*, and *Tilt End-On* Coordinations of N_2 Bound to the Co_3Mo_3N Surface

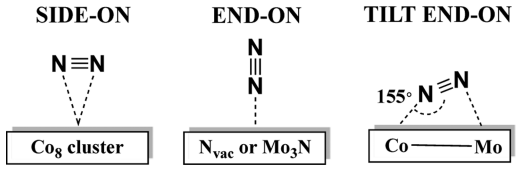

adsorption configurations for molecular nitrogen have been previously identified as *side-on* and *end-on*, based on an extensive collection of surface analytical studies.[33,36] *Side-on* and *end-on* adsorbed configurations for N_2, when it is adsorbed to nickel surfaces have also been found, where the *end-on* adsorption occurs either through a single surface atom on Ni(110) surfaces or in a *tilt end-on* configuration through two surface atoms on Ni(110) surfaces.[37] An *end-on* adsorbed configuration of N_2 as well as CO, which is isoelectronic, was found via X-ray emission spectroscopy (XES) and DFT calculations on Ni(100).[38] An *end-on* adsorbed configuration for N_2 has been found on cobalt clusters of the form $Co_n(N_2)^+$, where n = 8−17 using infrared photon dissociation (IRPD) spectroscopy and DFT calculations of the stretching frequency of the N−N bond.[39]

On the surface of Co_3Mo_3N (i.e., surface **C**), we have identified three adsorption configurations for N_2, which are shown in Scheme 2. For the eight adsorption sites, we placed N_2 either *side-on* or *end-on* at every site shown in Figure 3 and let it optimize without any restrictions. The adsorption energies for N_2 without (ΔE_{N2}) and with ($\Delta E_{H2,relax\text{-}D3}$) the inclusion of dispersion interactions via the DFT-D3 method and the optimized structure of the adsorbates (i.e., $r_{(H-H)}$, $r_{(M-H)}$, $a_{(M-H-H)}$) are presented in Table 3. The *side-on* configurations stayed either *side-on* or became a *tilt end-on* configuration during relaxation. This change in adsorption configurations was not observed for the *end-on* configuration, which remained *end-on* even after relaxation. This indicates that there is barrier for the end-on to side-on transformation. Adsorption at some sites would activate nitrogen, but dissociation such as in the case of H_2 was not observed, in accord with the large bond dissociation enthalpy of N_2 (i.e., 946 kJ/mol).

The various adsorption sites found had the following characteristics: **site 1** the nitrogen was adsorbed in a tilt end-on configuration to a molybdenum atom that was adjacent to a nitrogen-vacancy site (N_{vac}) with an adsorption energy of −59 kJ/mol but with only a small activation of the N−N bond. **Site**

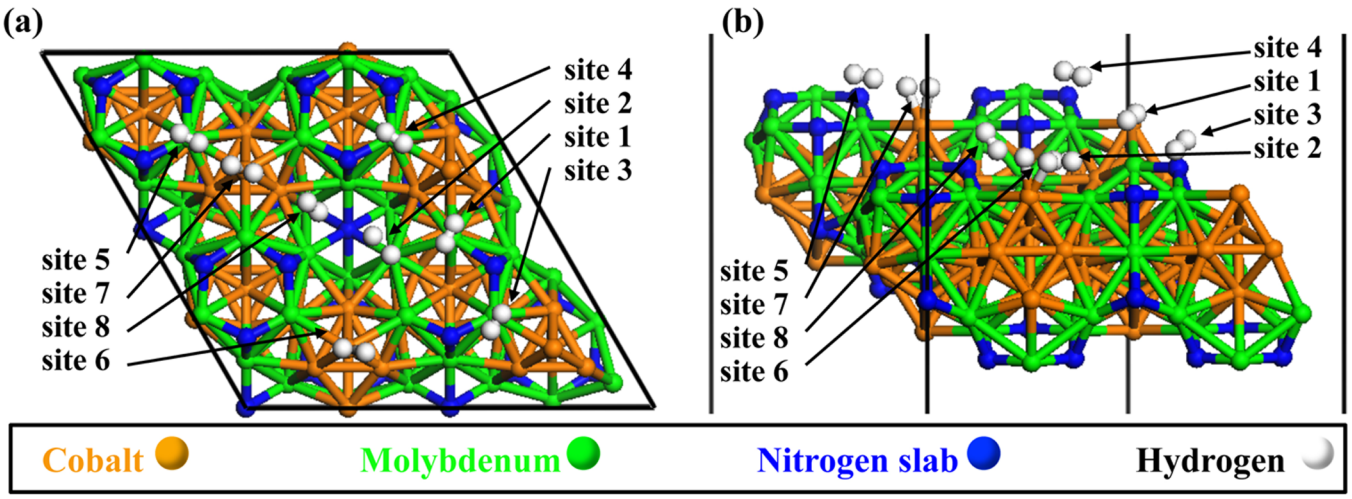

Figure 3. Symmetry unique adsorption sites for molecular nitrogen on Co_3Mo_3N surface **C** in the presence of a nitrogen vacancy (**site 1** and **2**) in (a) top view and (b) perspective view. Note that all adsorption sites are shown in one unit cell; however, the simulations results tabulated in Table 2 contained only one adsorbed nitrogen per 2 × 2 unit cell.

DOI: 10.1021/acs.jpcc.6b04748
J. Phys. Chem. C 2016, 120, 21390−21398

Table 3. Adsorption Energy (ΔE_{ads}) of N_2 Adsorbed to C Surface of Co_3Mo_3N, N−N Bond Length (r(N−N)), M−N Bond Length (r(M−N)), Tilt Angle (a(M−N−N)), Adsorption Site Composition, and % Elongation for Side-on Adsorption at Various Distinct Adsorption Sites on 2 × 2 Co_3Mo_3N (Surface C)[a]

property	site 1	site 2	site 3	site 4	site 5	site 6	site 7	site 8	units
ΔE_{ads}	−58.9	−19.6	59.8	−33.6	−44.3	−22.1	−18.7	79.3	kJ/mol
$\Delta E_{ads,D3\ relax}$	−58.9	−48.8	1.5	−29.9	−41.3	−38.2	−13.6	40.2	kJ/mol
r(N−N)	1.166	1.244	1.130	1.173	1.163	1.166	1.173	1.357	Å
a(M−N−N)	154	176	175	152	158	73	75	71	°
r(M−N)	1.753	1.930	2.398	1.820	1.754	2.001	1.971	1.928	Å
type	*tilt*	*end-on*	*end-on*	*tilt*	*tilt*	*side-on*	*side-on*	*side-on*	
bound to	N_{vac}	N_{vac}	MoN_3	$Co_{8\text{-top}}$	$Co_{8\text{-top}}$	$Co_{8\text{-top}}$	$Co_{8\text{-top}}$	$Co_{8\text{-side}}$	
N_2 activation[b]	4	11	1	5	4	4	5	21	%

[a]The *32e* and *16d* Wyckoff sites of the Co_8 in the bulk, have been denoted as $Co_{8\text{-top}}$ and $Co_{8\text{-side}}$ for the surface slabs, respectively. [b]Percent activation is defined as $[r(N_2,g) - r(N_2,ads)] \times 200/[r(N_2,g) + r(N_2,ads)]$.

2 was found to activate N_2, where it was bound *end-on* at the 3-fold hollow generated by the nitrogen vacancy. This site had the second largest % activation (i.e., 11%) for molecular nitrogen. **Site 3** N_2 was adsorbed in an *end-on* configuration on the Mo_3N framework with a weak adsorption energy (1.5 kJ/mol) due to the less metallic character of the Mo_3N framework. **Site 4−5** N_2 adsorbs in a *tilt end-on* at the *32e* Wyckoff site of the ($Co_{8\text{-top}}$) configuration with a 4−5% activation of the N−N bond and an adsorption energy of −30 to −41 kJ/mol. **Site 6−7** N_2 adsorbs in a *side-on* at the *32e* Wyckoff site ($Co_{8\text{-top}}$), with a 4−5% activation of the N−N bond. Interestingly we find a surface cavity on surface **C** of Co_3Mo_3N (**site 8**), at which there is the largest activation of N−N bond, 21%. This % activation is even larger than the activation that we have found at 5f sites on surface **B**, which was 19%, in a previous study.[13] Although the adsorption energy at this site maybe positive, if we take into account the entropy change for adsorption at 300 K, which is $-T\Delta S$= −58 kJ/mol, the adsorption free energy becomes −17 kJ/mol. To summarize, two activation sites for N_2 have been found (i) the first at nitrogen vacancies on the Mo_3N framework (i.e., **site 2**) and (ii) the second at surface cavities where it activated on a Co atom at the *16d* Wyckoff sites Co_8 (i.e., **site 8**, $Co_{8\text{-side}}$). The existence of two activation sides for nitrogen clearly suggests that there may be more than one ammonia synthesis mechanism occurring on Co_3Mo_3N catalysts. In the following section, we explain based on molecular orbital (MO) diagrams why these three adsorption configurations where found, based on the energy and spatial distribution of the frontier orbitals.

3.4. Interpretation of the Three N_2 Adsorption Configurations on Co_3Mo_3N.

It is intriguing that there are three different low-coverage adsorption configurations for N_2 on the surface of Co_3Mo_3N, which suggests that there are three different adsorbate−surface bonding interactions. We have calculated with MP2/cc-pVTZ the molecular orbitals (MOs) of N_2 in order to tentatively offer an interpretation of the three adsorption configurations found. The eigenvalues and eigenfunctions of these calculations are shown in Figure 4, which show that the ordering for the highest-occupied-molecular-orbitals (HOMO: $1\pi_u$), which has a π-symmetry is separated by only 0.7 eV from an MO with σ-symmetry (HOMO−1: $3\sigma_g$). Both these orbitals are expected to undergo bonding interactions. Because these MOs have their lobes pointing along directions perpendicular to the molecular axis (90°) of N_2 and along the molecular axis (180°), therefore bonding interactions are expected along these directions. Furthermore, these MOs are not expected to take any charge

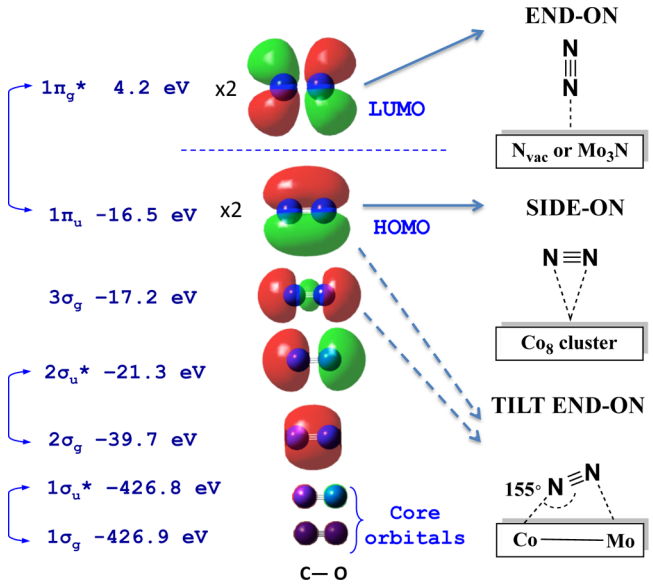

Figure 4. Molecular orbitals and their corresponding energies for N_2 calculated at MP2/cc-pVDZ level of theory, as well as how they correlate to the various adsorbed configurations of N_2.

from the metal atoms, but could possibly donate electron density in the form of π-donation and σ-donation, respectively. Morokuma[40] in an energy decomposition analysis (EDA) of the bonding in $(CO)_4Fe-CO$ and $(CO)_4Fe-N_2$ revealed equaly strong contributions from σ-donation and π-back-donation, results which however may differ for cobalt dimers in which a very strong M−M interaction is present.[41]

The lowest-unoccupied-molecular-orbital (LUMO: $1\pi^*_g$) has a degenarate pair of orbitals and is expected to accept electron density from filled d-states of the metal through the π-back-donation mechanism.[42] The symmetry of the highest occupied-molecular-orbital (LUMO: $1\pi_u$) is identical to that of CO(g), although there the lobes of the antibonding orbital are somewhat stronger on the carbon atom.[43] We have previously shown that carbon monoxide (CO) adsorbs on various d^7, d^8, and d^9 metal nanoclusters in a primarily *end-on* configuration[44,45] at an angle of a(M−C-O) = 180°. The existence of the end-on configuration was explained by a mechanism in which the filled d-states of the metal (that have π-symmetry) donate electron density into the empty antibonding state of CO and where the filled HOMO of CO which has σ-symmetry and resembles the HOMO−1 of N_2, undergoes mostly σ-repulsion. This was in agreement with previous theoretical[43,46] and X-ray

DOI: 10.1021/acs.jpcc.6b04748
J. Phys. Chem. C 2016, 120, 21390−21398

emission spectroscopy (XES) studies.[47,48] CO adsorbed in a tilt configuration has been previously found on Ag_n (n = 1 to 7), which was rationalized on the basis of better orbital overlap of tilt-CO with Ag_n-HOMO of σ-symmetry and of the linear end-on CO with Ag_n-HOMO of π-symmetry.[49] Furthermore, a tilt-CO was also found as a results of CO−CO repulsions[50,51] or adsorption at 4-fold hollow sites.[52] There have been many computational studies of the doping, support and NP-size effects on CO adsorption on various metal and their oxides[53−59] and as elementary reaction steps in catalytic reactions.[60−62] In a recent combined DFT and experimental study of the catalytic CO oxidation using bimetallic $M_xAu_{25-x}SC_2H_4Ph$ clusters, where M = Cu, Au, Ag, the following trend Cu > Au > Ag was found and interpreted as a result of a stronger metal-CO interaction in metals with a smaller covalent radius.[40,41,63] Based on these earlier studies and the results found here, we rationalize that the π-back-donation of electron density into the LUMO of both N_2 and CO is expected to result in a linear *end-on* adsorption.[64] The *tilt end-on* adsorption configuration of N_2 on Co_3Mo_3N has not been previously reported and is shown in Scheme 2. This is a well-defined adsorption configuration with a tilt angle equal to 155° in which the dihedral d(Co−Mo−N−N) of this bond is found to be 0. In the following section, we provide evidence that there are two bonding interactions that take place based on the sphere-in-contact model.[65] We have taken literature values for the atomic radius of the elements participating in the bonding and drawn to scale a sphere-in-contact model of the *tilt end-on* adsorption configuration for N_2 on Co_3Mo_3N. This is depicted in Figure 5

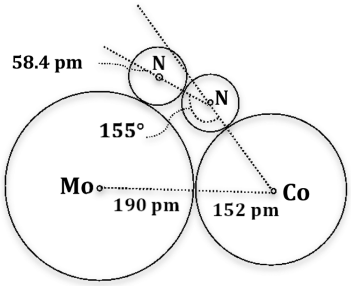

Figure 5. Sphere-in-contact model of *tilt end-on* adsorption configuration for N_2 on Co_3Mo_3N.

From the optimized structures presented in Table 2, we find that the tilt angle ranges between 152 and 158° with an average value at 155°. We have used the sphere-in-contact model to provide an explanation of the bonding in the *tilt end-on* configuration. In this model, each element is represented by its atomic radius. The atomic radius of nitrogen we can estimate from our DFT calculations (N: 58.4 pm) based on the average bond length of N_2 for the tilt end-on configuration, in excellent agreement with the double bond atomic radius obtained by fitting a set of atomic radius data of various elements (60 pm).[66] For the atomic radius of molybdenum and cobalt, we used literature values of 190 and 152 pm, respectively.[67] If we draw the bonding via a sphere-in-contact model as shown in Figure 5, we find that for a tilt angle of 155°, the spheres are in perfect contact, which indicates the presence of covalent bonding interactions, and that there is bonding both from the $3\sigma_g$ (HOMO−1) along the molecular axis of N_2 and the $1\pi_u$ (HOMO) perpendicular to the molecular axis of N_2. This orientation is such that it would additionally undergo interactions between filled d-states of the metal and antibonding $1\pi^*_g$ MO of N_2. The small percentage activation of the N−N bond indicates a potential bonding mechanism where π-back-donation and a tautochronous σ- and π-repulsion are present, which results in this unusual *tilt end-on* adsorbed configuration of N_2.

CONCLUSIONS

We present a dispersion-corrected DFT study of the adsorption and activation of molecular nitrogen and hydrogen on cobalt molybdenum nitride (111) surfaces to identify possible activation sites for ammonia synthesis. H_2 was found to adsorb both molecularly on the Mo_3N framework and dissociatively on Co_8 clusters or Mo_3 clusters that were exposed due to N-vacancies. N_2 was found to adsorb *side-on*, *end-on*, and in an unusual *tilt end-on* (155°) configuration, which is rationalized via MO diagrams and the sphere-in-contact model. We find that there are two possible activation sites for N_2. The first is a Mo_3 triangular cluster that resides at 3f nitrogen vacancies and the second is a surface cavity where N_2 is activated by the inner tetrahedral atom of the Co_8 cluster, the second being a more efficient activation site and a particular activation sites exposed only in Co_3Mo_3N surfaces with a surface composition of $CoMoN_{0.4}$.

AUTHOR INFORMATION

Corresponding Authors

*E-mail: c.zeinalipour-yazdi@ucl.ac.edu; Tel: +44 207-679-0312.

*E-mail: c.r.a.catlow@ucl.ac.uk; Tel: +44 207-235-2818.

Notes

The authors declare no competing financial interest.

ACKNOWLEDGMENTS

The authors acknowledge EPSRC funding (EP/L026317/1, EP/L02537X/1). Via our membership of the UK's HPC Materials Chemistry Consortium, which is funded by EPSRC (EP/L000202/1); this work used the ARCHER UK National Supercomputing Service (http://www.archer.ac.uk).

REFERENCES

(1) Jacobsen, C. J. H.; Brorson, M.; Sehested, T.; Teunissen, H.; Turnqvist, E. Process for the Preparation of Ammonia and Ammonia Synthesis Catalyst. US 6,235,676, 1999.

(2) Kojima, R.; Aika, K.-I. Cobalt Molybdenum Bimetallic Nitride Catalysts for Ammonia Synthesis: Part 1. Preparation and Characterization. *Appl. Catal., A* **2001**, *215*, 149−160.

(3) Jacobsen, C. J. H. Novel Class of Ammonia Synthesis Catalysts. *Chem. Commun.* **2000**, 1057−1058.

(4) Jacobsen, C. J. H.; Dahl, S.; Clausen, B. S.; Bahn, S.; Logadóttir, A.; Nørskov, J. Catalyst Design by Interpolation in the Periodic Table: Bimetallic Ammonia Synthesis Catalysts. *J. Am. Chem. Soc.* **2001**, *123*, 8404−8405.

(5) Boisen, A.; Dahl, S.; Jacobsen, C. J. H. Promotion of Binary Nitride Catalysts: Isothermal N_2 Adsorption, Microkinetic Model, and Catalytic Ammonia Synthesis Activity. *J. Catal.* **2002**, *208*, 180−186.

(6) Kojima, R.; Aika, K.-I. Cobalt Molybdenum Bimetallic Nitride Catalysts for Ammonia Synthesis. *Chem. Lett.* **2000**, *29*, 514−515.

(7) Kojima, R.; Aika, K.-I. Cobalt Molybdenum Bimetallic Nitride Catalysts for Ammonia Synthesis—Part 2. Kinetic Study. *Appl. Catal., A* **2001**, *218*, 121−128.

DOI: 10.1021/acs.jpcc.6b04748
J. Phys. Chem. C 2016, 120, 21390−21398

(8) Kojima, R.; Aika, K.-I. Cobalt Molybdenum Bimetallic Catalysts for Ammonia Synthesis—Part 3. Reactant Gas Treatment. *Appl. Catal., A* **2001**, *219*, 157−170.
(9) Nørskov, J. K.; Bligaard, T.; Logadóttir, A.; Bahn, S.; Hansen, L. B.; Bollinger, M.; Bengaard, H.; Hammer, B.; Sljivancanin, Z.; Mavrikakis, M.; et al. Universality in Heterogeneous Catalysis. *J. Catal.* **2002**, *209*, 275−278.
(10) McKay, D.; Gregory, D. H.; Hargreaves, J. S. J.; Hunter, S. M.; Sun, X. Towards Nitrogen Transfer Catalysis: Reactive Lattice Nitrogen in Cobalt Molybdenum Nitride. *Chem. Commun.* **2007**, 3051−3053.
(11) Hunter, S. M.; Gregory, D. H.; Hargreaves, J. S. J.; Richard, M. l.; Duprez, D.; Bion, N. A Study of $^{15}N/^{14}N$ Isotopic Exchange over Cobalt Molybdenum Nitrides. *ACS Catal.* **2013**, *3*, 1719−1725.
(12) Mckay, D.; Hargreaves, J. S. J.; Rico, J. L.; Rivera, J. L.; Sun, X.-L. The Influence of Phase and Morphology of Molybdenum Nitrides on Ammonia Synthesis Activity and Reduction Characteristics. *J. Solid State Chem.* **2008**, *181*, 325−333.
(13) Zeinalipour-Yazdi, C. D.; Hargreaves, J. S. J.; Catlow, C. R. A. Nitrogen Activation in a Mars-van Krevelen Mechanism for Ammonia Synthesis on Co_3Mo_3N. *J. Phys. Chem. C* **2015**, *119*, 28368−28376.
(14) Abghoui, Y.; Garden, A. L.; Hlynsson, V. F.; Bjorgvinsdottir, S.; Olafsdottir, H.; Skulason, E. Enabling Electrochemical Reduction of Nitrogen to Ammonia at Ambient Conditions Through Rational Catalyst Design. *Phys. Chem. Chem. Phys.* **2015**, *17*, 4909−4918.
(15) Michalsky, R.; Pfromm, P. H.; Steinfeld, A. Rational Design of Metal Nitride Redox Materials for Solar-Driven Ammonia Synthesis. *Interface Focus* **2015**, *5*, 20140084−10.
(16) Michalsky, R.; Avram, A. M.; Peterson, B. A.; Pfromm, P. H.; Peterson, A. A. Chemical Looping of Metal Nitride Catalysts: Low-Pressure Ammonia Synthesis for Energy Storage. *Chem. Sci.* **2015**, *6*, 3965−3974.
(17) Kresse, G.; Furthmüller, J. Efficient Iterative Schemes for *ab initio* Total-Energy Calculations Using a Plane-Wave Basis Set. *Phys. Rev. B: Condens. Matter Mater. Phys.* **1996**, *54*, 11169−11186.
(18) Kresse, G.; Hafner, J. *Ab initio* Molecular Dynamics for Liquid Metals. *Phys. Rev. B: Condens. Matter Mater. Phys.* **1993**, *47*, 558−561.
(19) Zhang, Y.; Yang, W. Comment on "Generalized Gradient Approximation Made Simple. *Phys. Rev. Lett.* **1998**, *80*, 890.
(20) Grimme, S.; Antony, J.; Ehrlich, S.; Krieg, H. A Consistent and Accurate ab initio Parametrization of Density Functional Dispersion Correction (DFT-D) for the 94 Elements H-Pu. *J. Chem. Phys.* **2010**, *132*, 154104.
(21) Frisch, M. J.; Trucks, G. W.; Schlegel, H. B.; Scuseria, G. E.; Robb, M. A.; Cheeseman, J. R.; Scalmani, G.; Barone, V.; Mennucci, B.; Petersson, G. A., et al. *Gaussian 09*, revision E.1; Gaussian Inc.: Wallingford CT, 2009.
(22) Woon, D. E.; Dunning, T. H., Jr. Gaussian Basis Sets for Use in Correlated Molecular Calculations. III. The Second Row Atoms, Al-Ar. *J. Chem. Phys.* **1993**, *98*, 1358−1371.
(23) Paier, J.; Marsman, M.; Hummer, K.; Kresse, G.; Gerber, I. C.; Ángyán, J. G. Screened Hybrid Density Functionals Applied to Solids. *J. Chem. Phys.* **2006**, *124*, 154709−154713.
(24) Paier, J.; Marsman, M.; Hummer, K.; Kresse, G.; Gerber, I. C.; Ángyán, J. G. Erratum: Screened Hybrid Density Dunctionals Applied to Solids. *J. Chem. Phys.* **2006**, *125*, 249901.
(25) Hunter, S. M. Molybdenum Nitrides: Structural and Reactivity Studies. PhD Thesis, University of Glasgow, 2012.
(26) Prior, T. J.; Battle, P. D. Superparamagnetism and Metal-Site Ordering in Quaternary Nitrides with the η-carbide Structure. *J. Mater. Chem.* **2004**, *14*, 3001−3007.
(27) Hunter, S. M.; Mckay, D.; Smith, R. I.; Hargreaves, J. S. J.; Gregory, D. H. Topotactic Nitrogen Transfer: Structural Transformation in Cobalt Molybdenum Nitrides. *Chem. Mater.* **2010**, *22*, 2898−2907.
(28) Waki, T.; Terazawa, S.; Tabata, Y.; Sato, K.; Kondo, A.; Kindo, K.; Nakamura, H. Observation of two Ferromagnetic Phases in Fe3Mo3N. *Phys. Rev. B: Condens. Matter Mater. Phys.* **2014**, *90*, 014416.
(29) Jackson, S. K.; Layland, R. C.; zur Loye, H. C. The Simultaneous Powder X-ray and Neutron Diffraction Refinement of two Eta-Carbide Type Nitrides, Fe_3Mo_3N and Co_3Mo_3N, Prepared by Ammonolysis and by Plasma Nitridation of Oxide Precursors. *J. Alloys Compd.* **1999**, *291*, 94−101.
(30) Lewis, E. A.; Le, D.; Murphy, C. J.; Jewell, A. D.; Mattera, M. F. G.; Liriano, M. L.; Rahman, T. S.; Sykes, E. C. H. Dissociative Hydrogen Adsorption on Close-Packed Cobalt Nanoparticle Surfaces. *J. Phys. Chem. C* **2012**, *116*, 25868−25873.
(31) Nakhaei Pour, A.; Keyvanloo, Z.; Izadyar, M.; Modaresi, S. M. Dissociative Hydrogen Adsorption on the Cubic Cobalt Surfaces: A DFT Study. *Int. J. Hydrogen Energy* **2015**, *40*, 7064−7071.
(32) Zeinalipour-Yazdi, C. D.; Efstathiou, A. M. Preadsorbed Water-Promoted Mechanism of the Water-Gas Shift Reaction. *J. Phys. Chem. C* **2008**, *112*, 19030−19039.
(33) Rao, C. N. R.; Ranga Rao, G. Nature of Nitrogen Adsorbed on Transition Metal Surfaces as Revealed by Electron Spectroscopy and Cognate Techniques. *Surf. Sci. Rep.* **1991**, *13*, 223−263.
(34) Freund, H.-J.; Bartos, B.; Messmer, R. P.; Grunze, H.; Kuhlenbeck, H.; Neumann, M. The Adsorption of N2 on Fe(111): Angle Resolved Photoemission and Theoretical Model Studies. *Surf. Sci.* **1987**, *185*, 187−202.
(35) Mortensen, J. J.; Hansen, L. B.; Hammer, B.; Nørskov, J. K. Nitrogen Adsorption and Dissociation on Fe(111). *J. Catal.* **1999**, *182*, 479−488.
(36) Tsai, M.-C.; Ship, U.; Bassignana, I. C.; Küppers, J.; Ertl, G. A Vibrational Spectroscopy Study on the Interaction of N_2 with Clean and K-promoted Fe(111) Surfaces: π-bonded Dinitrogen as Precursor for Dissociation. *Surf. Sci.* **1985**, *155*, 387−399.
(37) Horn, K.; Dinardo, J.; Eberhardt, W.; Freund, H. J.; Plummer, E. W. The Adsorption of N2: Chemisorbed on Ni(110) and Physisorbed on Pd(111). *Surf. Sci.* **1982**, *118*, 465−495.
(38) Nilsson, A.; Hasselström, J.; Föhlisch, A.; Karis, O.; Pettersson, L. G. M.; Nyberg, M.; Triguero, L. Probing chemical bonding in adsorbates using X-ray emission spectroscopy. *J. Electron Spectrosc. Relat. Phenom.* **2000**, *110*−*111*, 15−39.
(39) Dillinger, S.; Mohrbach, J.; Hewer, J.; Gaffga, M.; Niedner-Schatteburg, G. Infrared Spectroscopy of N_2 Adsorption on Size Selected Cobalt Cluster Cations in Isolation. *Phys. Chem. Chem. Phys.* **2015**, *17*, 10358−10362.
(40) Morokuma, K. Molecular Orbital Studies of Hydrogen Bonds. III. C═O···H−O Hydrogen Bond in $H_2CO···H_2O$ and $H_2CO···2H_2O$. *J. Chem. Phys.* **1971**, *55*, 1236−1244.
(41) Gámez, J. A.; Tonner, R.; Frenking, G. Gallium Halides as Alternative Ligands to CO and N_2 in Transition Metal Complexes: A Bonding Analysis. *Organometallics* **2010**, *29*, 5676−5680.
(42) Blyholder, G. Molecular Orbital View of Chemisorbed Carbon Monoxide. *J. Phys. Chem.* **1964**, *68*, 2772−2777.
(43) Sung, S. S.; Hoffmann, R. How carbon monoxide bonds to metal surfaces. *J. Am. Chem. Soc.* **1985**, *107*, 578−584.
(44) Zeinalipour-Yazdi, C. D.; Cooksy, A. L.; Efstathiou, A. M. CO adsorption on Transition Metal Clusters: Trends from Density Functional Theory. *Surf. Sci.* **2008**, *602*, 1858−1862.
(45) Zeinalipour-Yazdi, C. D.; Cooksy, A. L.; Efstathiou, A. M. A Diffuse Reflectance Infrared Fourier-Transform Spectra and Density Functional Theory Study of CO Adsorption on Rh/gamma-Al_2O_3. *J. Phys. Chem. C* **2007**, *111*, 13872−13878.
(46) Bagus, P. S.; Nelin, C. J.; Bauschlicher, C. W. Bonding of CO to Metal Surfaces: A New Interpretation. *Phys. Rev. B: Condens. Matter Mater. Phys.* **1983**, *28*, 5423−5438.
(47) Fohlisch, A.; Nyberg, M.; Hasselstrom, J.; Karis, O.; Pettersson, L.; Nilsson, A. How carbon monoxide adsorbs in different sites. *Phys. Rev. Lett.* **2000**, *85*, 3309−3312.
(48) Föhlisch, A.; Nyberg, M.; Bennich, P.; Triguero, L.; Hasselström, J.; Karis, O.; Pettersson, L. G. M.; Nilsson, A. The bonding of CO to metal surfaces. *J. Chem. Phys.* **2000**, *112*, 1946−1958.

DOI: 10.1021/acs.jpcc.6b04748
J. Phys. Chem. C 2016, 120, 21390−21398

(49) Acioli, P. H.; Burkland, S.; Srinivas, S. An exploration of the potential energy surface of the seven atom silver cluster and a carbon monoxide ligand. *Eur. Phys. J. D* **2012**, *66*, 215.
(50) Ko, E. I.; Madix, R. J. Effects of adsorbed Carbon and Oxygen on the Chemisorption of H_2 and CO on Mo(100). *Surf. Sci.* **1981**, *109*, 221−238.
(51) Minot, C.; Van Hove, M. A.; Biberian, J.-P. Theory of CO Adsorption on MgO(100): The Influence of Intermolecular Interactions on the CO Orientation. *Surf. Sci.* **1996**, *346*, 283−293.
(52) Rochana, P.; Wilcox, J. A Theoretical Study of CO Adsorption on FeCo(100) and the Effect of Alloying. *Surf. Sci.* **2011**, *605*, 681−688.
(53) Akbarzadeh, H.; Yaghoubi, H.; Shamkhali, A. N.; Taherkhani, F. CO adsorption on Ag nanoclusters supported on carbon nanotube: A molecular dynamics study. *J. Phys. Chem. C* **2014**, *118*, 9187−9195.
(54) Akbarzadeh, H.; Yaghoubi, H.; Shamkhali, A. N.; Taherkhani, F. CO adsorption on Ag nanoclusters supported on carbon nanotube: A molecular dynamics study. *J. Phys. Chem. C* **2014**, *118*, 9187−9195.
(55) Hartshorn, H.; Pursell, C. J.; Chandler, B. D. Adsorption of CO on supported gold nanoparticle catalysts: A comparative study. *J. Phys. Chem. C* **2009**, *113*, 10718−10725.
(56) Mahmoodinia, M.; Åstrand, P. O.; Chen, D. Influence of Carbon Support on Electronic Structure and Catalytic Activity of Pt Catalysts: Binding to the CO Molecule. *J. Phys. Chem. C* **2016**, *120*, 12452−12462.
(57) Morrow, B. H.; Resasco, D. E.; Striolo, A.; Nardelli, M. B. CO adsorption on noble metal clusters: Local environment effects. *J. Phys. Chem. C* **2011**, *115*, 5637−5647.
(58) Shetty, S.; Strych, S.; Jansen, A. P. J.; van Santen, R. A. Theoretical investigation of CO adsorption on Rhn (n = 3−13) clusters1. *Can. J. Chem.* **2009**, *87*, 824−831.
(59) McKee, W. C.; Patterson, M. C.; Huang, D.; Frick, J. R.; Kurtz, R. L.; Sprunger, P. T.; Liu, L.; Xu, Y. CO Adsorption on Au Nanoparticles Grown on Hexagonal Boron Nitride/Rh(111). *J. Phys. Chem. C* **2016**, *120*, 10909−10918.
(60) Gasper, R. J.; Ramasubramaniam, A. Density Functional Theory Studies of the Methanol Decomposition Reaction on Graphene-Supported Pt_{13} Nanoclusters. *J. Phys. Chem. C* **2016**, *120*, 17408.
(61) Zhang, Q.; Mamtani, K.; Jain, D.; Ozkan, U.; Asthagiri, A. CO Poisoning Effects on FeNC and CN_x ORR Catalysts: A Combined Experimental-Computational Study. *J. Phys. Chem. C* **2016**, *120*, 15173−15184.
(62) Kumari, N.; Haider, M. A.; Agarwal, M.; Sinha, N.; Basu, S. Role of Reduced CeO_2(110) Surface for CO_2 Reduction to CO and Methanol. *J. Phys. Chem. C* **2016**, *120*, 16626.
(63) Li, W.; Liu, C.; Abroshan, H.; Ge, Q.; Yang, X.; Xu, H.; Li, G. Catalytic CO Oxidation Using Bimetallic M_xAu_{25-x} Clusters: A Combined Experimental and Computational Study on Doping Effects. *J. Phys. Chem. C* **2016**, *120*, 10261−10267.
(64) Zeinalipour-Yazdi, C. D.; van Santen, R. A. Coverage-Dependent Adsorption Energy of Carbon Monoxide on a Rhodium Nanocluster. *J. Phys. Chem. C* **2012**, *116*, 8721−8730.
(65) Zeinalipour-Yazdi, C.; Pullman, D.; Catlow, C. The Sphere-in-Contact Model of Carbon Materials. *J. Mol. Model.* **2016**, *22*, 40.
(66) Pyykkö, P.; Atsumi, M. Molecular Double Covalent Radii for Elements. *Chem. - Eur. J.* **2009**, *15*, 12770−12779.
(67) Clementi, E.; Raimondi, D. L.; Reinhardt, W. P. Atomic Screening Constants from SCF Functions. *J. Chem. Phys.* **1963**, *38*, 2686−2689.

DOI: 10.1021/acs.jpcc.6b04748
J. Phys. Chem. C 2016, 120, 21390−21398